Innovative Infrastructure Solutions (2026) 11:129
https://doi.org/10.1007/s41062-026-02524-1

Dynamic lane configuration and cooperative autonomous vehicles for improving travel time on smart roads: a case study

Marco Guerrieri[1] · **Luigi Sanfilippo**[2]

Received: 14 November 2025 / Accepted: 17 January 2026
© The Author(s) 2026

Abstract

To reduce congestion on urban and suburban road networks, specific capacity-enhancing strategies must be implemented, either through physical and structural interventions or by adopting appropriate traffic regulation systems. The introduction of smart roads and autonomous vehicles (CAVs) offers new opportunities to enhance road functionality by adjusting capacity to fluctuating traffic demand over time. Among these strategies is the Dynamic Lane Configuration (DLC), which enables the dynamic adjustment of the number of lanes by modifying their original number and width, without compromising road safety in traffic flows composed of CAVs. This article presents the results of a study conducted on an urban arterial road in Italy, which was reconfigured by increasing the number of lanes and simultaneously reducing their width. Travel time and space mean speed were derived through the analysis of TomTom big data, and macroscopic fundamental diagrams (MFDs) were obtained, along with travel time functions, in the case of manually driven vehicles. A simplified traffic engineering closed-form model was subsequently developed to evaluate the effects of implementing the DLC system on the selected road, with a view toward its potential future transformation into a smart road accommodating different market penetration levels of CAVs. The proposed approach is then tested through several traffic analyses, which highlight the potential benefits of the novel traffic control strategy.

Keywords Mobility big data · Dynamic lane configuration · Smart road · Cooperative autonomous vehicles · Travel time

Abbreviations

c_T	Capacity of the carriageway in the basic condition, DLC inactive (pc/h)
c'_T	Capacity of the carriageway in the modified configuration, DLC active (pc/h)
CAVs	Connected and autonomous vehicles
DLC	Dynamic lane configuration
FCD	Floating car data
HDVs	Human-driven vehicles
k_i	Vehicle density of the road section i (pc/km)
k_c	Critical density (pc/km)
k_j	Jam density (pc/km)
k_{lim}	Desirable limit density value (pc/km)
k_w	Weighted vehicle density at the road network under consideration (pc/km)
l_i	Length of the road section i (m)
L	Total length of the road under consideration (m)
LDD	Loop detector data
LCFs	Link congestion functions
LOS	Level of service
MFD	Macroscopic fundamental diagram
MPL	Market penetration level of CAVs in the traffic flow (%)
q_i	Flow rate of the road section i (pc/h)
q_w	Weighted flow rate at the road network under consideration (pc/h)
TT	Travel time (s)
T_0	Minimal travel time (s)
TTI	Travel time index

✉ Marco Guerrieri
marco.guerrieri@unitn.it

Luigi Sanfilippo
luigi.sanfilippo@unipa.it

[1] Department of Civil, Environmental and Mechanical Engineering, University of Trento, via Mesiano 77, 38123 Trento, Italy

[2] Department of Engineering, University of Palermo, viale delle Scienze, 90144 Palermo, Italy

Published online: 19 February 2026

TT_{ph}	Mean travel time during peak hours (s)
TT_{ffs}	Mean travel time during free-flow conditions (s)
x	Degree of saturation (flow-to-capacity ratio)
VDFs	Volume-delay functions
v_f	Free-flow speed in the basic condition, DLC inactive (km/h)
v_f'	Free-flow speed in the modified configuration, DLC active (km/h)
v_i	Vehicle space mean speed of the road section i (km/h)
V_{max}	Imposed speed of CAVs (km/h)
v_w	Weighted vehicle space mean speed at the road network under consideration (km/h)
α	Ratio between practical capacity travel time and free flow time in the BPR formula
β	Steepness of the curve in the BPR formula (rate of change of average travel speed from free-flow regime to congested conditions)
γ	Critical density ratio (critical density of the modified carriageway configuration/critical density of the original configuration)
δ	Ratio of the capacity values (capacity of the modified carriageway configuration/capacity of the original configuration)
ε	Number of lanes ratio (number of lanes of the modified carriageway configuration/number of lanes of the original configuration)
λ	Number of lanes per carriageway in the basic configuration, DLC inactive
λ'	Number of lanes per carriageway in the modified configuration, DLC active
σ	Free-flow speed ratio (free-flow speed of the modified carriageway configuration/free-flow speed of the original configuration)
τ_m	Time headway between pairs of vehicles in the traffic streams (s)

Introduction

Traffic congestion has emerged or worsened in many cities worldwide, negatively impacting urban mobility — affecting both daily travel routines and the efficiency of emergency operations [1]. Additionally, it intensifies issues related to travel safety, energy consumption, and air pollution. Understanding where, when, and to what extent congestion occurs should guide the development of effective mitigation strategies. Therefore, congestion indicators with high spatial and temporal resolution are essential for informed policy-making [2]. To mitigate the effects of oversaturation that often occurs on existing roads due to high traffic demand levels, road management agencies often implement costly physical interventions aimed at widening the road cross-section to increase capacity. However, these interventions are costly and often impractical, also for technical reasons. For this reason, special traffic flow regulation systems, such as Managed lanes (e.g., dynamic peak-hour lanes, additional lanes, high-occupancy vehicle lanes, and bus lanes), are used. Managed lanes' operations comprise a set of traffic strategies designed to enhance roadway capacity or to modify its configuration in order to prioritize a specific transportation mode (e.g., buses, taxis, or high-occupancy vehicles) or mitigate recurring congestion. In the latter case, the increase in capacity is typically achieved by redefining the transverse profile within the existing roadway boundaries. Various technical options can be implemented, such as reducing lane widths and temporarily or permanently utilising the hard shoulder as a running lane [3]. The hard shoulder running (HSR) strategy has proven to be an effective measure to alleviate freeway traffic congestion. This strategy dynamically opens and closes the hard shoulder in response to current traffic conditions. When traffic flow is relatively low or special requirements arise, the hard shoulder reverts to its original emergency lane function [4]. This type of traffic regulation system has the advantage of not requiring modifications to the road platform or changes to the lane dimensions. Still, it requires significant investments in technology and is generally combined with VSL systems. However, compared to platform expansion HSR traffic control system often achieves increased capacity with lower investment costs and acceptable safety conditions. Some road management agencies are also experimenting with alternative traffic management systems on urban arterials. Some of these systems involve increasing the number of lanes while maintaining the same road platform; this approach involves using narrower-than-usual lanes without employing a dynamic system [5, 6]. Currently, this approach could lead to a higher accident risk. In fact, in general, sufficiently wide lanes and shoulders are associated with lower accident rates [7]. In any case, the ever-increasing presence of driving assistance systems, and above all, the future introduction of CAVs (defined here as automated vehicles with an operating cooperative adaptive cruise control system) will make it possible to overcome potential safety problems resulting from limited lanes and shoulders. Connected and Automated Vehicles (CAVs) offer the capability to enhance road safety while simultaneously mitigating traffic congestion, fuel consumption, and both air and noise pollution [8]. Through advanced sensors [9, 10], data sharing and accurate motion planning, these systems enable more efficient traffic control—particularly within complex or high-conflict zones such as intersections, roundabouts, and merging sections of roadways. CAVs could find a set of non-dominated shortest paths in stochastic transportation

networks, potentially offering benefits in terms of travel time [11]. The foundation of automated mobility lies in the cooperative interaction among CAVs, made possible by vehicle-to-vehicle and vehicle-to-smart road connectivity. Such cooperation supports the development of control algorithms that jointly optimize travel time, energy efficiency, and passenger comfort, all while rigorously maintaining safety constraints. Conversely, a transportation network composed solely of Human-Driven Vehicles (HDVs) operates according to individualistic, vehicle-centred decision-making, where each driver acts competitively rather than collaboratively with others on the road. Thanks to the automated driving system and a specific routing framework that integrates traffic sensor data augmentation and deep learning techniques to improve the reliability of route and lane selection, CAVs will be able to maintain precise and consistent trajectories [12, 13–16]. Therefore, in the future, it will be possible to use lanes of a much smaller size than the current ones, even for roads travelled at high speed. Furthermore, a dynamic configuration could also be introduced by adjusting the number of lanes and their width as needed, resulting in a corresponding dynamic increase or decrease in capacity during the service life. This would allow vehicles to flow in several parallel lanes that can vary in number and configuration over time based on traffic demand. The concept of Dynamic Lane was originally proposed in [9]. Specifically, when traffic demand increases, the number of lanes can be increased by reducing their width; conversely, for low traffic demand, the number of lanes can be reduced and their width increased. This approach can help maintain optimal infrastructure service levels and ensure acceptable transit times. However, research on the Dynamic Lane Configuration (DLC) is mainly focused on HDVs. Advancements in connected and autonomous vehicle (CAV) technology can generate innovative solutions to the DLC strategy for highways and urban roads.

This article presents and addresses the topic of dynamic lane configuration in a case study of the city of Palermo. The first part of the article compares service levels, speeds, and travel times resulting from the introduction of an additional lane within the carriageway (simultaneously reducing the width of all lanes). To achieve this goal, Mobility Big Data (MBD) from TomTom was analysed (four weeks in October 2019 and four weeks in October 2024). Afterwards, the effects of introducing Dynamic Lane Configuration are then estimated for different percentages of CAVs in vehicle flows, also proposing a possible control strategy for the traffic regulation system, starting from the operational condition of the road when it is in operation. The traffic stream composed of CAVs is regarded as an artificially designed fluid; its collective properties are programmable and optimizable predominantly in terms of maximum speeds (V_{max}) that vehicles should not exceed.

In summary, the main innovations and contributions of this article are as follows:

a) studying the traffic effect generated by the introduction of an additional lane in the carriageway of an existing arterial road with a contextual width reduction of all lanes;
b) analyse the potential benefits of a dynamic lane configuration system on existing roads and smart roads [17];
c) develop a traffic engineering model able to predict travel time under the activation of the dynamic lane configuration
d) examining how different percentages of CAVs in traffic flows could impact the performance of the system in terms of travel time.

The rest of the paper is structured as follows. Sect. "Theory MFD and Travel Time models" briefly describes some key factors on the Macroscopic Fundamental Diagram (MFD) and Travel Time models. Sects. "Methodology and case study" explain the methodology and the case study. Sect. "Macroscopic fundamental diagrams and travel time model deduction" describes the MFD and TT models deduction for the analysed case under consideration. Sect. "Dynamic Lane configuration in CAVs environment" examines the Dynamic Lane configuration in the case of CAVs environment with a simplified traffic model for the deduction of TT and results of traffic analyses for different flow rate conditions and Market Penetration Levels (MPLs) of CAVs. Conclusions, limitations of the study and research perspectives are given in Sect. "Conclusions".

Theory: MFD and travel time models

From a macroscopic perspective, the key traffic variables that define traffic flow conditions are flow q (vehicles per unit time), space mean speed v, and vehicle density k (vehicles per unit length of lane). Under uninterrupted and steady-state traffic conditions, these variables are related through the fundamental traffic equation: $q = k \cdot v$. This relationship is commonly illustrated using the fundamental diagram (FD), which typically expresses speed as a function of flow $v = v(q)$. When the macroscopic traffic flow variables are calculated as averages at the road network level or for a very long segment of a single road, the relationships that occur between q, v, and k are referred to as the Macroscopic Fundamental Diagram (MFD). Therefore, the MFD has similar characteristics to the FD, but rather than concerning a road cross-section, it relates space-averaged speed, flow

and density for long road segments or road networks. The macroscopic fundamental diagram (MFD) can be utilised for various purposes because it is a relatively simple method by which traffic engineers can calculate the effects of traffic control. The original idea of MFD was first proposed by Godfrey [2], although its basic theory was developed in 2007 by Geroliminis and Daganzo [3, 4], who demonstrated the usefulness of MFD for analysing the traffic conditions of Yokohama City. In recent times, MFD has been extensively applied to evaluate the impacts of traffic control on urban road system performance [5, 6]. Moreover, studies on arterial and motorway networks have been investigated using MFDs [7–9]. At a road network level, the macroscopic traffic variables can be defined as follows:

$$q_w = \frac{\sum_i q_i \cdot l_i}{\sum_i l_i} \quad (1)$$

$$k_w = \frac{\sum_i k_i \cdot l_i}{\sum_i l_i} \quad (2)$$

$$v_w = \frac{\sum_i v_i \cdot l_i}{\sum_i l_i} \quad (3)$$

in which q_i, k_i, v_i, and l_i represent flow, density, space mean speed, and length values related to the road section i belongs to the network under consideration, and q_w, k_w, and v_w are the weighted homologous traffic variables.

As noted in [7, 8, 10], the Macroscopic Fundamental Diagram (MFD) represents an aggregate characteristic of a road network's structure that remains independent of traffic demand patterns, such as origin–destination matrices. This makes MFDs a valuable tool for forecasting how various traffic management strategies might impact overall network performance. To derive the MFD, several primary estimation methods can be employed, including the Loop Detector Data (LDD) method, radar, a video image detection system [18], and the Floating Car Data (FCD) method [11, 12]. Together with the three macroscopic traffic variables (v, q and k), another one is added, which is widely used in traffic engineering, namely the Travel Time (TT) [19, 20]. TT is a key measure of effectiveness in evaluating urban arterials. For a generic vehicle, the travel time TT_i is the time required to pass a road section or a network of a given length. Denoting with $L = \sum_i l_i$ the length of the road network into consideration (or the length of the urban arterial), the following simple relationship links the TT of a sample n of vehicles with their average speed in space: $v = L/TT$. Therefore, in technical applications, the MFD can also be usefully employed for some specific evaluations of TT values. This is a very interesting aspect because in several traffic engineering applications, it is essential to establish how travel time along a road segment changes based on traffic volume q (i.e. the so-called link cost function). More precisely, in traffic assignment methods, road capacity constraints on travel time are specified using volume-delay functions (VDFs) or link congestion functions (LCFs) [21]. VDFs are mathematical equations used to account for the effect of increased traffic volumes on travel time. To derive the VDF for a given road segment, concurrent speed and traffic count surveys are typically carried out across multiple survey periods [22]. A practical link cost function typically incorporates free-flow travel time, link-specific delays, and intersection delays [23]. Among the most widely used link cost functions are those developed by the Bureau of Public Roads (BPR), as well as the Davidson, Akçelik, and conical delay functions. The most used VDFs are listed in Table 1. Among these, the best known is the Bureau of Public Roads model (i.e. BPR formula).

The BPR function, in particular, is extensively applied in transportation planning due to its simple mathematical structure, reliance on readily measurable input data, and consistent accuracy in various scenarios. The BPR function is a polynomial function that relates traffic volume q to roadway capacity c. It includes two key parameters: alpha (α) and beta (β). The alpha parameter serves as a scaling factor, while beta determines the shape of the function, influencing how sharply travel time increases with congestion. Parameter α represents the ratio of travel time per unit distance at practical capacity to the free-flow travel time, while β governs the rate at which congestion impacts travel time (TT). A higher value of β indicates a more sudden onset of congestion, as travel times escalate more steeply once the road approaches its capacity. Analysing the distribution of travel times over an extended period (such as a year) is essential for assessing the effectiveness of road infrastructure and traffic management systems, as well as understanding the impact of various policies and strategies on their performance. In addition, travel time can be used to assess road reliability [27]. In general, reliability can be defined as "the probability that a component or system will perform a required function for a given period of time when used under stated operating conditions. It is the probability of non-failure over time"[28]. In transportation engineering, travel time reliability (TTR) can be defined as the probability that a traveller can successfully complete a trip within a specified time [29]. In addition, a variety of performance metrics have been developed to capture travel time variability, among others, including the following [30]: Travel Time Index (TTI), Planning Time Index (PTI), Buffer Index (BI), Misery Index (MI), and Modified Misery Index. Table 2 summarises the TTR measures that were developed and utilized in past studies [31].

Table 1 Description of the most used VDF models

Model name	Equations	Model parameters
Bureau of public roads [24]	$TT = T_0 \cdot \left[1 + a\,(x)^{\beta}\right]$	T_0: minimal travel time $x = \frac{q}{c}$ α: ratio between practical capacity travel time and free flow time β: steepness of the curve (rate of change of average travel speed from free-flow regime to congested conditions)
Conical volume-delay function ([25])	$TT = T_0 \cdot \left[2 + \sqrt{\alpha^2 (1-x)^2 + \beta^2} - \alpha \cdot (1-x) - \beta\right]$	T_0: minimal travel time $x = \frac{q}{c}; ? = \frac{2?-1}{2?-2}$ α: any number greater than 1
Modified davidson – [21]	$TT = \begin{cases} T_0 \cdot \left(1 + j\frac{x}{1-x}\right); x \leq \mu \\ T_0 \cdot \left(1 + j\frac{x}{1-x} + j\frac{(x-\mu)}{(1-\mu)^2}\right); x > \mu \end{cases}$	T_0: minimal travel time $x = \frac{q}{c}$ μ: user-selected proportion, often set to 0.85 – 0.95 J: delay parameter (related to land use or type of land surrounding the link)
Akcelik Delay Function [26]	$TT = T_0 \cdot \left(1 + 0.25 \cdot r_f \cdot \left[x - 1 + \left((x-1)^2 + 8\frac{j_A \cdot x}{c \cdot T_0 \cdot r_f}\right)^{0.5}\right]\right)$	T_0: minimal travel time $x = \frac{q}{c}; r_f = \frac{T_f}{T_0}; j_A = \frac{2c}{T_f}(T_c - T_0)^2$ T_f: analysis period T_c: travel time at capacity

Methodology and case study

Mobility Big Data is transforming traffic management and urban transport planning, thanks to the ability to collect vast amounts of data, including in real-time. According to [39] Willumsen, this information comes from various sources, such as mobile signals, public transport smart cards, mobile applications, GPS, and Wi-Fi/Bluetooth technologies. Mobile data, collected through mobile networks or GPS applications on smartphones, tracks user movements in real-time. Smart cards, on the other hand, enable the monitoring of public transport demand, while mobile apps utilise GPS data to optimise routes and reduce congestion. GPS systems and Wi-Fi/Bluetooth technologies are crucial for collecting data on vehicles and people in motion, especially in densely populated urban areas. Willumsen (2021) [39] suggests that combining these data with traditional methods, such as travel surveys, helps reduce costs and improve the quality of analysis, providing a comprehensive view of urban mobility dynamics. The use of Big Data enables the tracking of changes in travel behaviours, learning from quasi-experiments, and developing new transportation demand models. GPS data, in particular, is widely used in mobility analysis. These data are collected through GPS devices installed on vehicles or smartphones, enabling the precise determination of an object's location as it moves. They provide crucial information on routes, travel times, traffic congestion, and disruptions. Navigation apps use this data to suggest alternative routes in real-time, optimising transport efficiency and reducing traffic. Additionally, GPS data are crucial for studying travel habits, identifying the most frequently used routes, and enhancing transportation services. Companies like TomTom International BV manage this data through complex algorithms, continuously mapping the information received from mobile devices, vehicles, and corporate fleets. The data are stored in TomTom's servers, where they are real-time mapped and made available via a web portal. Several case studies highlight the effectiveness of Big Data in mobility. In the field of highway engineering, for instance, Salvo et al. [40] used real-time TomTom data to analyse the impact of floods on mobility in Palermo, developing emergency management scenarios and traffic control strategies. Pozzoni et al. [41] utilised GPS data to evaluate the impact of infrastructure changes in Bologna, noting a shift in traffic towards surrounding roads following a tactical urbanism intervention. Current research demonstrates the importance of mobility Big Data, particularly GPS data, in optimising traffic management, enhancing transport planning, and addressing challenges in urban infrastructure. The use of these technologies continues to evolve, promising to significantly transform how cities and transportation systems are designed and managed.

Table 2 Most used TTR measures (adapted from [31])

Travel time reliability measure	Equation / definition	Agency/author
Travel Time Index (TTI)	average travel time / free-flow travel time	–
90th/95th percentile travel times	90th/95th percentile travel times	FHWA [32]
Buffer Index (BI)	(95th percentile time − average travel time) / average travel time × 100%	FHWA [32]
Coefficient of Variation (COV)	Standard deviation / average travel time	Pu [33]
Frequency of Congestion (FOC)	Frequency of trips exceeding a threshold value	FHWA [32]
Misery Index (MI)	(Average travel rate (Top 20% trips) / average travel rate) − 1	Lomax et al. [34]
Planning Time Index (PTI)	95th percentile travel time / free-flow travel time	FHWA [33]
Present Variation	(Standard deviation / average travel time) × 100%	California Transportation Plan [35]; Lomax et al.[34] NCHRP Report 618 [36]
Skew of Travel Time Distribution*	$\lambda^{skew} = (T_{90} - T_{50}) / (T_{50} - T_{10})$	Van Lint and Van Zuylen [37]
Standard Deviation	Standard deviation	Dowling et al. [38]; Pu [33]
Variability Index	Difference in peak-period confidence intervals/difference in off-peak-period confidence intervals	Lomax et al. [34]
Width of Travel Time Distribution	$\lambda^{width} = (T_{90} - T_{50}) / (T_{50} - T_{10})$	Van Lint and Van Zuylen [37]

*T_{90}, T_{50} and T_{10} denote the 90th percentile travel time, the 50th percentile travel time and the10th percentile travel time, respectively

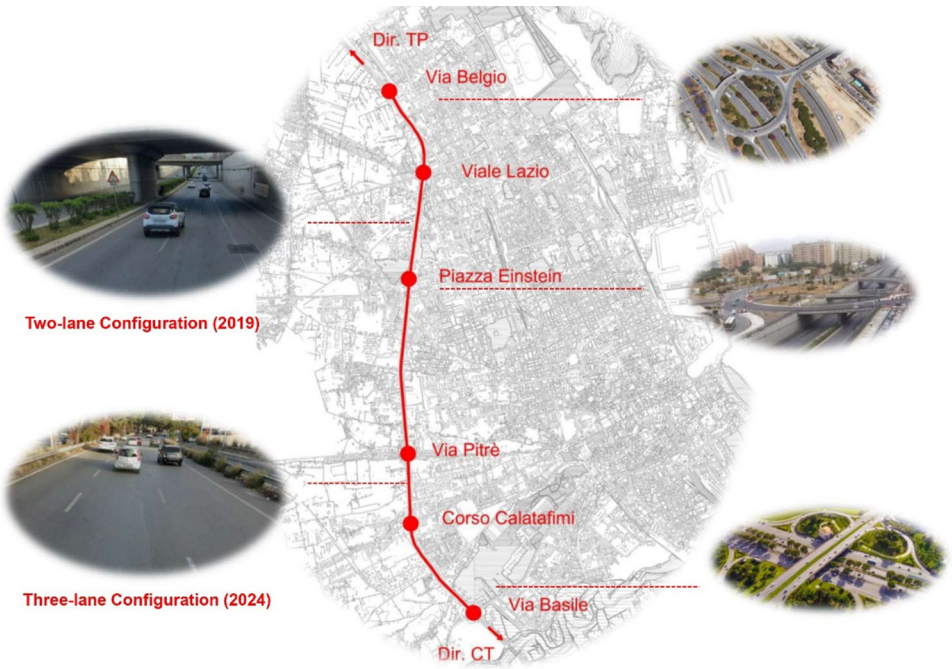

Fig. 1 Section of "Viale Regione Siciliana" under analysis

In this research, the speed and travel time data were collected using Tom-Tom data on the urban arterial corridor "Viale Regione Siciliana" in Palermo (Italy). The selected test bed section was originally a four-lane divided road. In fact, before April 2019, the road initially had two lanes in each direction, each approximately 4.5 m wide, and a shoulder approximately 3 m wide. In the new configuration, a third lane was introduced. Therefore, this new configuration features three 3-m lanes (narrower than the original ones) per carriageway, resulting in a total of six lanes, and a 2.5-m shoulder (Fig. 1).

Speed data and travel times were calculated for four weeks in October 2019 and four weeks in October 2024 to estimate the impact of adding an additional lane per carriageway:

Period n° 1: from 2019–09-30 to 2019–10-27;
Period n° 2: from 2024–09-30 to 2024–10-27.

In both periods, data from Saturdays and Sundays were excluded from the analysis.

Figure 2 reports the number of vehicles observed in the various daily time slots for which the variables of interest (travel time and speed) were deduced using all the recorded and available TomTom data. The number of vehicles is obviously much lower than the overall flow for the same time

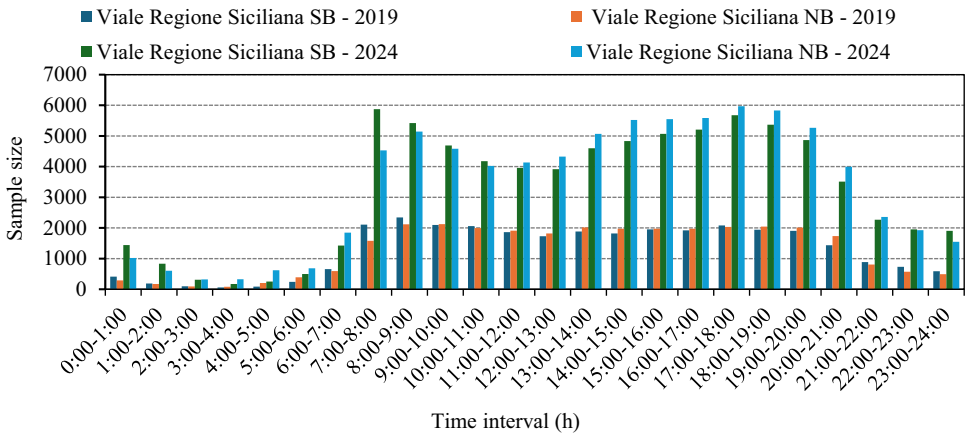

Fig. 2 Sample floating car data for the two periods considered in the study

Table 3 Flow values. (Dir. CT = Catania Direction; Dir TP = Trapani direction)

Junction	Time interval	Dir. CT		Dir. TP		Dir. CT + Dir. TP
		Q (pc/h)	P (%)	Q (pc/h)	P (%)	q_{Tot} (pc/h)
Svincolo Basile	08.00–09.00	929	10.01	1706	9	2635
	09.00–10.00	859	9.2	736	12	1595
	10.00–11.00	754	14.33	559	4	1313
Corso Calatafimi	08.00–09.00	1713	4.67	5582	4	7294
	09.00–10.00	1333	6.53	4967	4	6299
	10.00–11.00	1331	5.19	5193	6	6524
Via Pitrè	08.00–09.00	2042	9.84	2976	4	5018
	09.00–10.00	1394	9.25	2148	4	3542
	10.00–11.00	1104	9.97	1960	4	3063
Piazza Einstein	08.00–09.00	1656	13.71	6050	12	7706
	09.00–10.00	811	13.33	5592	10	6402
	10.00–11.00	860	15.12	4165	12	5025
Viale Lazio	08.00–09.00	1553	9.66	2231	12	3784
	09.00–10.00	1374	11.5	1931	15	3305
	10.00–11.00	1257	11.38	1482	16	2738
Via Belgio	08.00–09.00	846	13	1504	12	2350
	09.00–10.00	656	8.85	1532	11	2187
	10.00–11.00	868	13.72	1279	11	2147

slot. Furthermore, the 2024 sample is larger than the 2019 sample, as it has been possible to obtain greater coverage of floating car data with respect to a given flow q in recent years (Fig. 2). In any case, the sample for the year 2019 is statistically significant enough to make a reliable estimate of speeds and travel times. The equivalent traffic flows (q) and the percentage of heavy vehicles (p) relating to the morning rush hour were deduced from the Urban Traffic Plan of Palermo [42]. In particular, we considered three hourly time intervals: 08:00–09:00, 09:00–10:00, and 10:00–11:00. These intervals are organised into five different sections, each homogeneous in terms of flow rate. Each section is identified by the name of the nearest junction (Table 3). Along the examined 6.3 km-long road section, there is also a traffic light intersection and a pedestrian crossing. As can be seen from the results summarized in these Figures, space mean speeds and travel times, are significantly different for the two directions. This is due to numerous factors, including the various locations of the entrance and exit lanes from the urban arterial, the number and position of lateral intersections, and others.

Several service quality indicators have been developed, with the primary goal of evaluating the service level of a road infrastructure. The current criteria used to determine the Level of Service (LOS) of highways and arterial roads are based on vehicle density. However, density is not easily or directly measurable, nor is it readily available in the field for road operators to assess the operational performance of road infrastructure, unlike data on traffic volume, speed, and travel times [24]. Moreover, speed and travel times are easily understood by both users and road operators. Figures 3, 4, 5, 6, 7, 8, and 9 shows a comparison of the effects of introducing the third lane on travel times and average speeds on both carriageways for different time slots. In this regard,

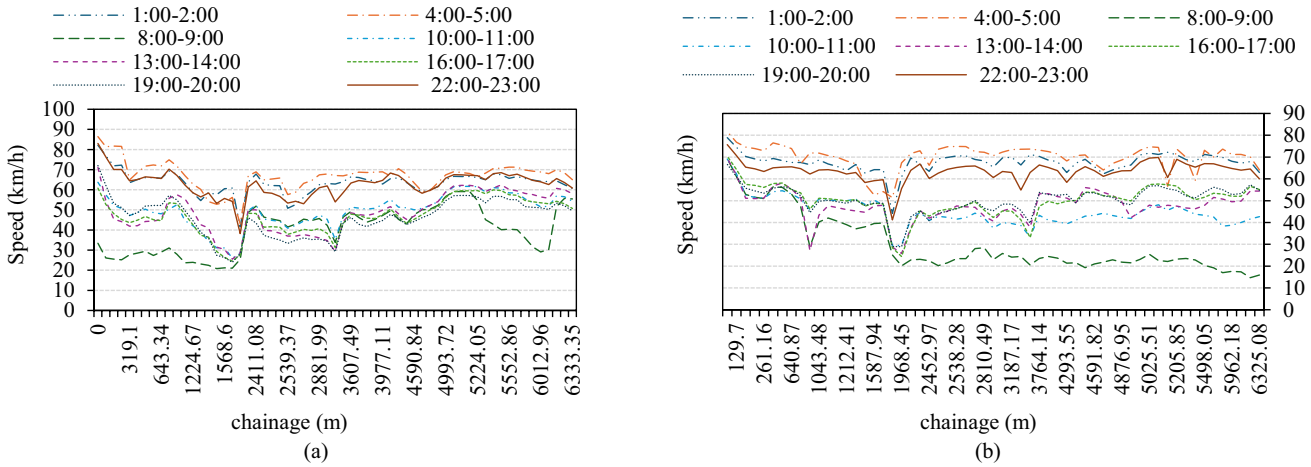

Fig. 3 Space mean speed, year 2019. **a** SB (TP → CT); **b** NB. (CT → TP)

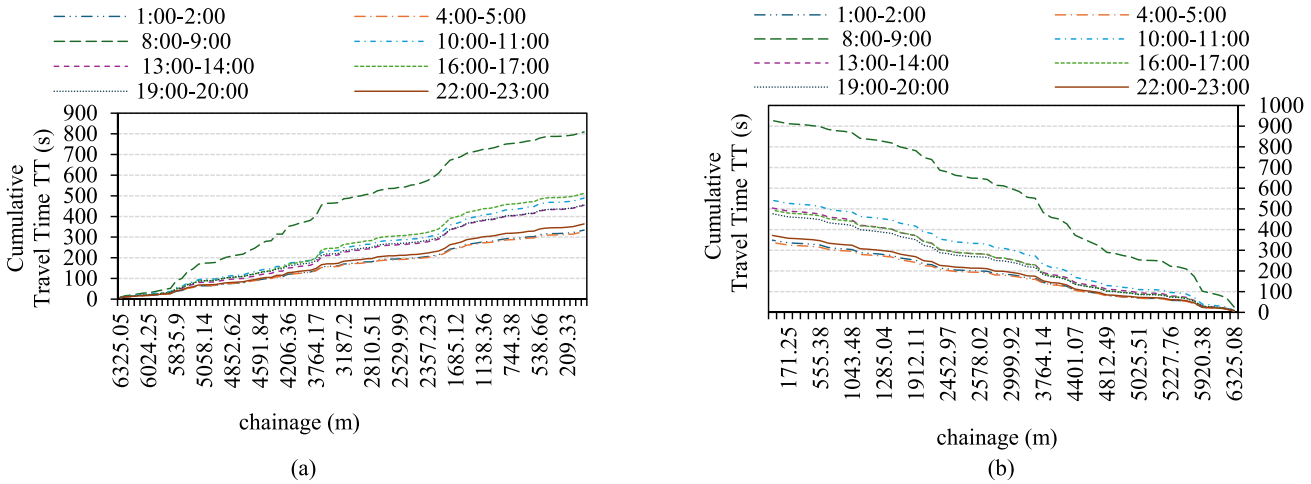

Fig. 4 Cumulative Travel Time, year 2019. **a** SB (TP → CT); **b** NB. (CT → TP)

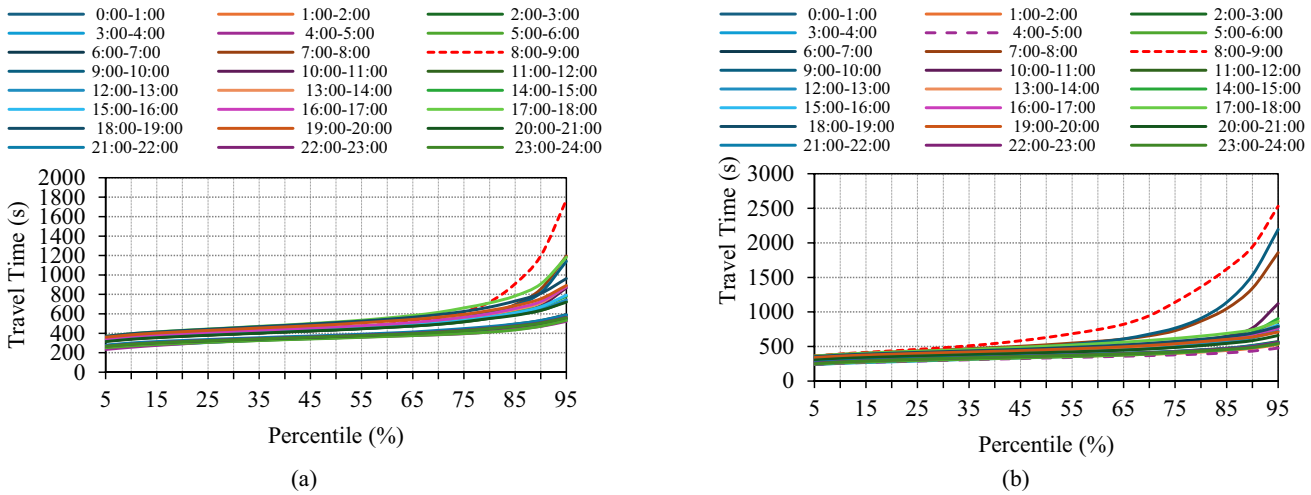

Fig. 5 Percentile Travel Time, year 2019. **a** SB (TP → CT); **b** NB. (CT→ TP)

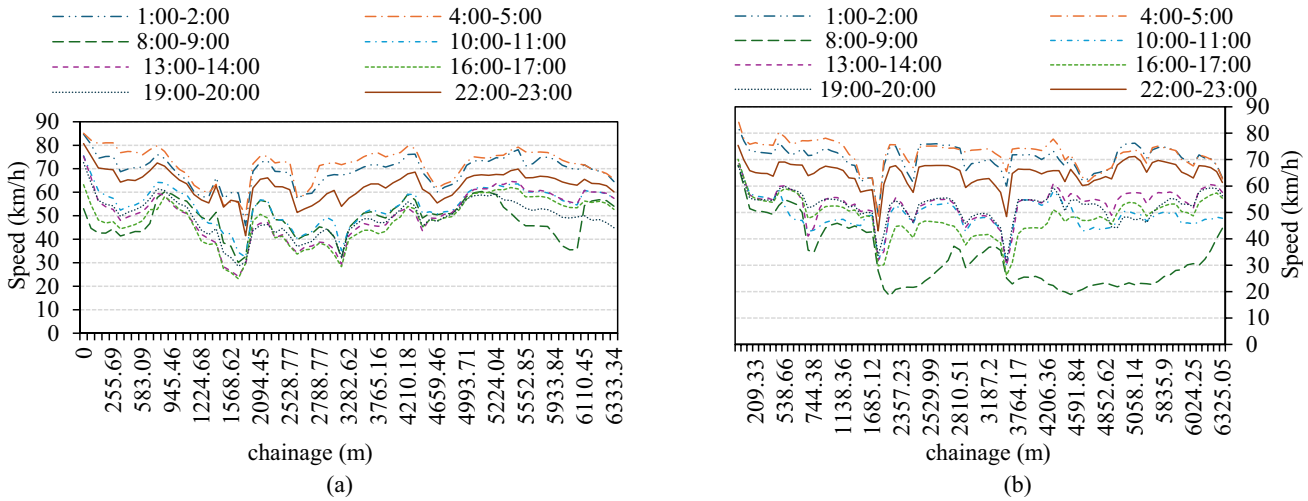

Fig. 6 Space mean speed, year 2024. **a** SB (TP → CT); **b** NB. (CT → TP)

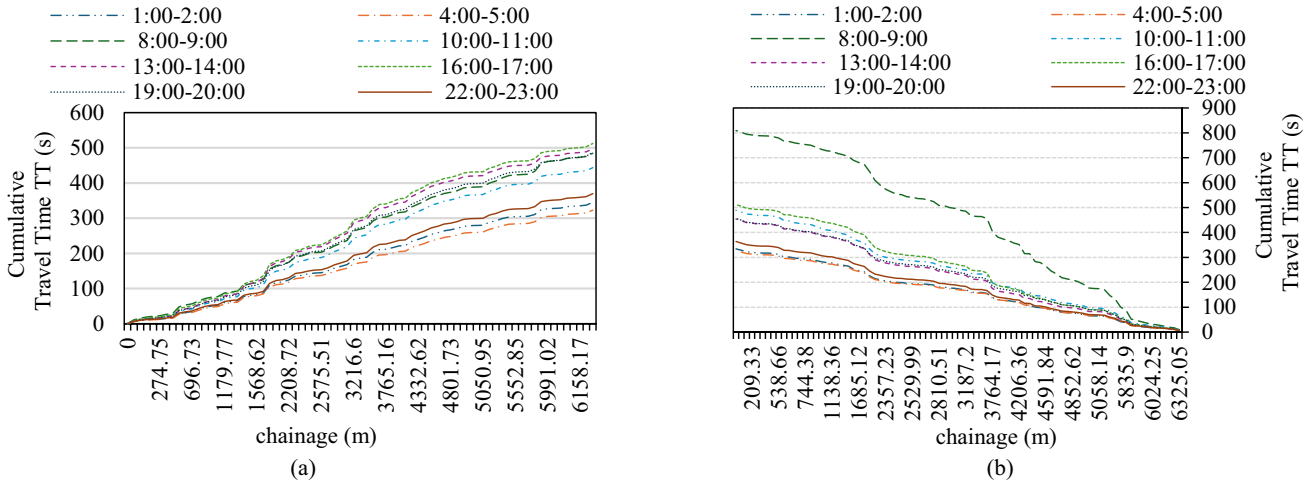

Fig. 7 Cumulative Travel Time, year 2024. **a** SB (TP → CT); **b** NB. (CT → TP)

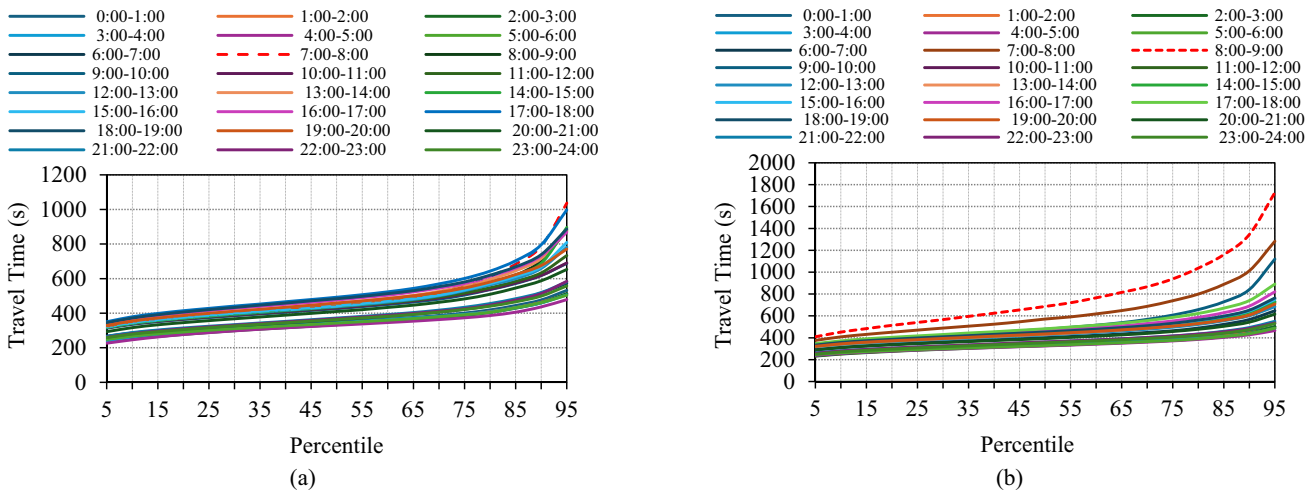

Fig. 8 Percentile Travel Time, year 2024. **a** SB (TP → CT); **b** NB. (CT → TP)

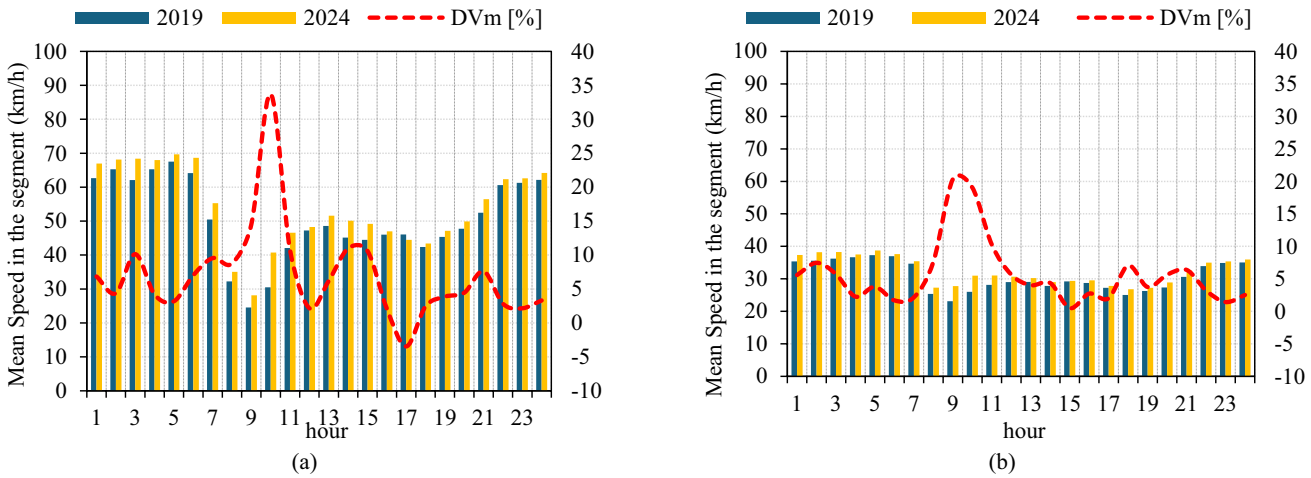

Fig. 9 Means speed comparison year 2019 vs year 2024 and percentage variation (DVm). SB (TP → CT); **b** NB. (CT → TP)

several studies have demonstrated that the free-flow speed (FFS) decreases as the lane width decreases. For instance, according to the HCM 2010, if the lane width of freeways is reduced by 0.3 m (1 ft) from the base condition width of 3.65 m, free flow speed (v_f) decreases by about 3.1 km/h compared to the base condition. Lane widths as narrow as 3.0 m can significantly reduce the v_f, by up to 10.6 km/h [5, 43]. In the case study, being an urban arterial road with a speed limit of 70 km/h, the reduction in lane width does not determine any reduction in speed even in free-flow conditions, which actually seems to increase slightly during the nighttime slots (Fig. 9). Moreover, Fig. 9 immediately highlights the advantages in terms of space mean speed, especially during rush hour. In fact, increases in the mean speed can reach around 35% during peak traffic periods. These benefits are also deductible in terms of service levels (LOS). In particular, Table 4 presents the LOS calculated using the HCM method [5] for each section of the analysed road during the three morning time slots, based on the flow rates specified in Table 3. For the calculation of the LOS according to the speed levels derived in free flow conditions (night time slots), a free flow speed $v_f = 70$ km/h was assumed for the original 2019 scenario (2 lanes for each carriageway) and $v_f = 75$ km/h for the modified 2024 scenario (3 lanes for each carriageway) (cf. Figs. 3 and6). In fact, according to the *Highway Capacity Manual* [44], the Free-Flow Speed v_f of a road segment is defined as the theoretical speed that would occur when both traffic density and flow rate are zero. Since this condition cannot exist in reality, the HCM recommends estimating v_f by measuring spot speeds and averaging the values observed under low-flow conditions, such as those that may occur during nighttime hours. The LOS benefit is achieved at all time slots and for all road sections, which is particularly evident during traffic peaks. This benefit is obviously linked to the increase in roadway capacity and the resulting lower degree of saturation achieved with the same traffic flow.

However, although the new configuration brings clear advantages in terms of average speeds and therefore travel time, significant congestion is still observed. In this research, the travel time index (TTI) is used (cf. Table 2). TTI is defined as follows:

$$\mathrm{TTI} = \frac{\mathrm{TT_{ph}}}{\mathrm{TT_{ffs}}} \tag{4}$$

where TT_{ph} is the Mean Travel Time During Peak Hours and TT_{ffs} is the Mean Travel Time During Free-flow Conditions.

Figure 10 highlights that the TTI always remains relatively high for both carriageways, reaching a value of 2 in almost all roads and exceeding a value of 3 in some road segments. This means that TT during congestion (i.e. in the peak hour) is 300% higher than in non-peak hours (Fig. 11).

Macroscopic fundamental diagrams and travel time model deduction

For the urban arterial under consideration, the free-flow speed is comparable to the average speed observed during the 4:00–5:00 a.m. time slot, relating to road sections free of disturbances due to pedestrian crossings (Piazzale Giotto—pedestrian intersections on call and Via Perpignano), however, little used (pedestrian flows are almost absent). Once the free-flow speed v_f is defined, the lane capacity c can also be estimated according to the HCM manual [45]. Therefore, the following values are deduced in this study: a) $v_f = 70$ km/h, $c = 1900$ veh/h for the year 2019; b) $v_f = 75$ km/h, $c = 1950$ veh/h for the year 2024. There are numerous traffic models described in the literature, each with distinct forms

Table 4 LOS variations

	Section	Hour 8:00–9:00				Hour 9:00–10:00				Hour 10:00–11:00			
		2 lanes		3 lanes		2 lanes		3 lanes		2 lanes		3 lanes	
		k (pc/km/ln)	LOS	k (pc/km/ln)	LOS	k (pc/km/ln)	LOS	k (pc/km/ln)	LOS	k (pc/km/ln)	LOS	k (pc/km/ln)	LOS
SB Carriageway (Dir. CT)	Via Belgio—Viale Lazio	7.2	B	4.4	A	7.2	B	4.4	A	7.4	B	4.6	A
	Viale Lazio—Piazza Einstein	14.1	C	8.8	B	14.1	C	8.8	B	11.7	C	7.3	B
	Piazza Einstein—Via Pitrè	17.6	D	11.0	B	17.6	D	11.0	B	9.4	B	5.9	A
	Via Pitrè—Corso Calatafimi	21.9	D	13.6	C	21.9	D	13.6	C	11.8	C	7.4	C
	Corso Calatafimi—Svincolo Basile	16.4	D	10.2	B	16.4	D	10.2	B	13.0	C	8.1	B
NB Carriageway (Dir. TP)	Via Belgio—Viale Lazio	12.7	C	7.9	B	12.7	C	7.9	B	10.7	B	6.7	B
	Viale Lazio—Piazza Einstein	21.1	D	13.1	C	21.1	D	13.1	C	14.6	C	9.1	B
	Piazza Einstein—Via Pitrè	90.7	E	47.7	F	90.7	E	47.7	F	50.1	F	29.8	F
	Via Pitrè—Corso Calatafimi	28.0	E	16.9	D	28.0	E	16.9	D	17.7	D	11.0	B
	Corso Calatafimi—Svincolo Basile	66.0	E	37.4	F	66.0	E	37.4	F	68.4	F	38.5	F

and mathematical formulations [22], including single and multi-regime models.

In this research, the classic Greenshields model was employed to derive the Macroscopic Fundamental Diagram (MFD), due to its inherent simplicity, which requires only two traffic variables: the free-flow speed (v_f) and the jam density (k_j). In the Greenshields model the Speed-density ($v = v(k)$) and Flow – density ($q = q(k)$) relationships are:

$$v(k) = v_f \cdot \left(1 - \frac{k}{k_j}\right) \tag{5}$$

$$q(k) = k \cdot v_f \cdot \left(1 - \frac{k}{k_j}\right) = v_f \cdot \left(k - \frac{k^2}{k_j}\right) \tag{6}$$

in which v_f is the free-flow speed, k_j the jam density, v the space mean speed and q the flow.

In this model, the following relationships can be deduced: $k_c = 2 \cdot c/v_f$, $k_j = 2\ k_c$, $c = ½\ k_c \cdot v_f$, where k_c is the critical density. Denoting c_T as the capacity of the carriageway, we obtain the parameters for model calibration.

a) Configuration of two lanes per carriageway (traffic data of the year 2019)

- Traffic variables for each lane: $k_c = 54$ pc/km/lane; $k_j = 108$ pc/km/lane;
- Traffic variables for the carriageway: $k_c = 108$ pc/km/carr; $k_j = 217$ pc/km/carr;

b) Configuration of three lanes per carriageway (traffic data of the year 2024)

- Traffic variables for each lane: $k_c = 52$ pc/km/lane; $k_j = 104$ pc/km/lane;
- Traffic variables for the carriageway: $k_c = 156$ pc/km/carr; $k_j = 312$ pc/km/carr;

The following figures compare the calibrated Greenshields traffic flow model for the two configurations under analysis. Given the method by which these graphs were obtained, they should be understood as macroscopic flow diagrams, allowing us to evaluate traffic conditions along the entire stretch of road, rather than just on a single section.

It should be noted that in the pre-existing scenario (year 2019), where each carriageway has two lanes, the measured flow rates theoretically lead to excessive roadway oversaturation. Indeed, the capacity of the carriageway is around 3,800 pc/h, while the measured flows in some cases exceed 6,000 pc/h (see Table 3). This apparent anomaly is explained by the fact that, in certain circumstances, road users disregard signage requirements and move in more

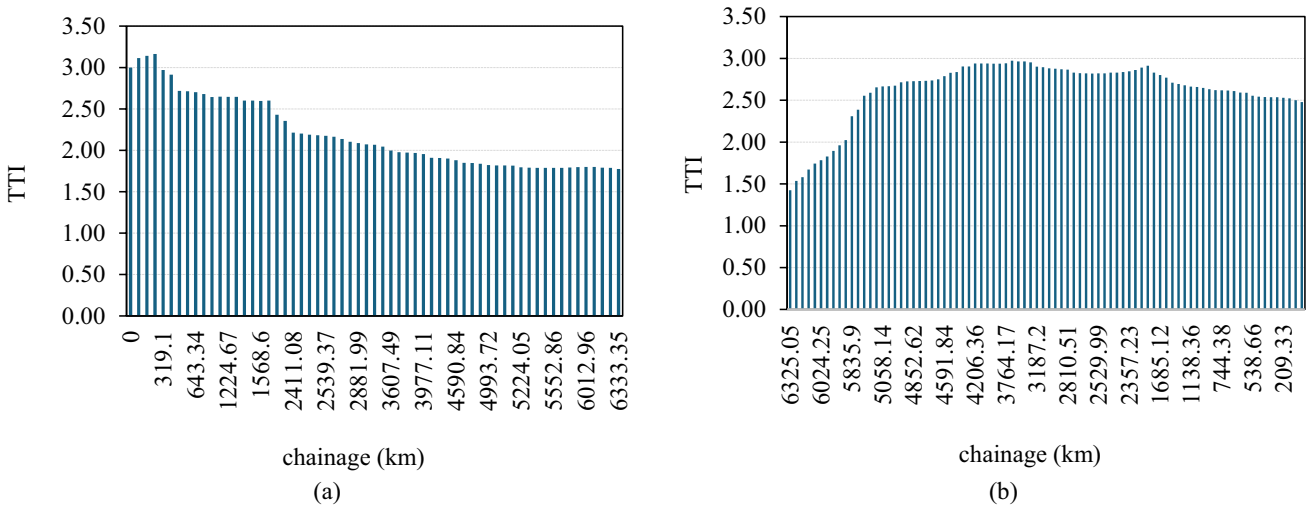

Fig. 10 Travel Time Index (TTI)—**a** SB (TP → CT); **b** NB. (CT → TP)

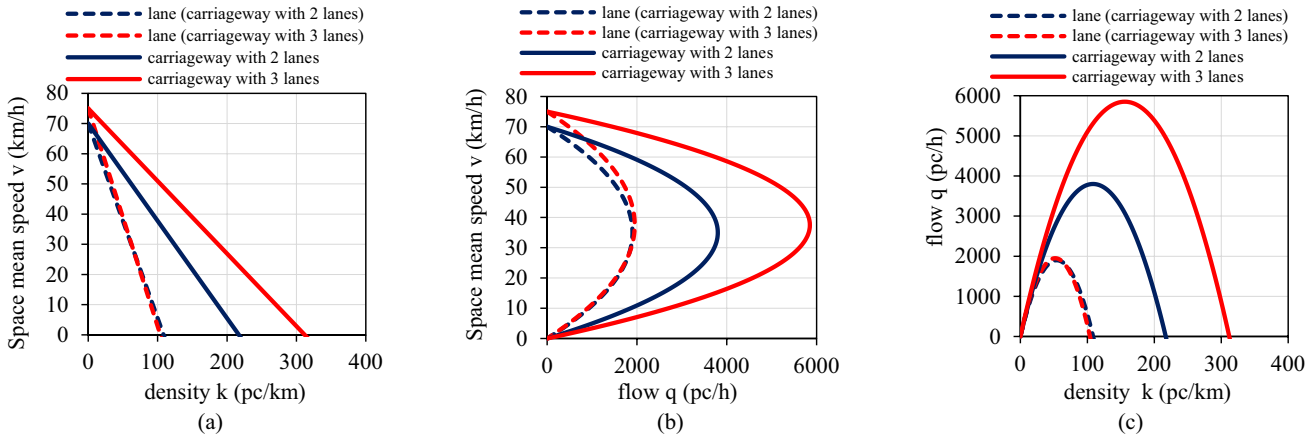

Fig. 11 Macroscopic fundamental diagram per the lane and carriageway

than two lanes. In other words, it's as if drivers' behaviour tended to optimise road capacity. In general terms, the relationships that exist between the mean travel time TT and the space mean speed v are:

$$v = \frac{n \cdot L}{\sum_{i=1}^{n} TT_i} \tag{7}$$

$$TT = \frac{L}{v} = \frac{\sum_{i=1}^{n} TT_i}{n} \tag{8}$$

where v is the space mean speed, L is the road segment length, TT_i is the observed travel time of the i-th vehicle, and n is the total number of travel times measured (i.e. the sample size), and TT is the mean travel time of all observed vehicles. It is evident that the TT_i values, and therefore the average TT values, are closely related to the degree of saturation x = q/c of the road. Various VDF models have been developed over time to assess a relationship that adequately correlates the TT with the values of q and c, and therefore of x = q/c. According to the BPR model, the travel time is proportional to the degree of saturation of the road, as shown in the equation:

$$TT = T_0 \left[1 + \alpha \left(\frac{q}{c}\right)^{\beta}\right] \tag{9}$$

where TT is the travel time of road segment (s) at a flow q level, T_0 is the free-flow travel time (s);q is the average traffic flow on road segment (veh/h), c is the capacity of road segment (veh/h); q/c is the degree of saturation and α and β are model parameters. The boundary conditions of the BPR function are as follows: for q = 0 veh/h, $TT = T_0$ and for q = c, $TT = T_0 [1 + \alpha]$. It is helpful to highlight that the BPR function has limitations. First, for the BPR function to represent oversaturation conditions, the model should be calibrated considering "oversaturation" demand (capacity volume plus residual queue). Furthermore, Eq. 9

is deterministic. However, the TT can vary for the same flow rate depending on the circumstances [46]. In the BPR function, the coefficients α and β are estimated from field data. Generally, lower α (0.8–0.9) and higher β (2.5–3.0) are used for heavily congested roads, while higher α (1.2–1.5) and lower β (1.5–1.8) are used for urban roads. For highways, β is usually set to 2.0 [47]. The conventional calibration of the BPR model relies on statistical methods that use either observed speeds or travel times as inputs for the corresponding volume data. After the least squares optimization technique [48], the following relationship has been obtained:

$$TT = 325.5428 \cdot \left[1 + 0.615944\left(\frac{q}{c}\right)^{1.4985}\right] \quad (10)$$

Dynamic lane configuration in CAVs environment

The number of autonomous and connected vehicles is expected to continue rising in the near future. However, many vehicles are already equipped with various advanced driver-assistance systems (ADAS), including cruise control and lane-keeping assists, designed to help keep a vehicle within its lane on the road. By exploiting these driving assistance systems and smart road technologies, it is possible to consider introducing a new traffic control system called dynamic lane configuration (DLC) [49] (Fig. 12), or lane-free traffic, whereby vehicles are not bound to fixed traffic lanes but may drive anywhere on the road carriageway [50]. Analogous types of traffic regulation systems have also been designed and simulated for road intersections, particularly for novel smart and self-regulating roundabout types (i.e., COM-Roundabout [51] and SSF-Roundabout [52]), even in the presence of CAVs [53–55]. DLC is a traffic regulation system in which the number of lanes at each road section can be dynamically adjusted in response to a certain level of demand that varies in space and time. DLC can include the hard shoulder running system and can be considered an extension of this well-known concept in terms of intelligence. In the DLC system, the width of the lanes can also be dynamically varied, allowing a greater number of lanes to be inserted on the same roadway than those originally in operation. The expected benefit is similar to that previously examined for the case study. However, in DLC systems, the influence of different percentages of CAVs must be taken into consideration [50].

In this section, the effect of introducing the dynamic lane and varying percentages of CAVs is considered using a new, simple traffic model derived from observations of the operating conditions of the road under analysis. The number of lanes per carriageway is defined as $\lambda = 2$ in the basic configuration (2 lanes per carriageway, with DLC inactive) and $\lambda' = 3$ in the modified configuration (3 lanes per carriageway). The free-flow speeds in the basic and modified configurations are denoted by v_f and v_f', respectively, while the corresponding carriageway capacities are denoted by c_T and c'_T. The following relations can be written:

$$c_T = \left(\frac{k_c \cdot v_f}{2}\right) \cdot \lambda \quad (11)$$

$$c'_T = \left(\frac{k'_c \cdot v'_f}{2}\right) \cdot \lambda' \quad (12)$$

$$\delta = \frac{c'_T}{c_T} = \frac{k'_c \cdot v'_f}{k_c \cdot v_f} \cdot \frac{\lambda'}{\lambda} = \gamma \cdot \sigma \cdot \varepsilon \quad (13)$$

where: $\gamma = \frac{k'_c}{k_c}$, $\sigma = \frac{v'_f}{v_f}$ and $\varepsilon = \frac{\lambda'}{\lambda}$.

In the previous equations δ, γ, σ, and ε stand for capacity increase, critical density ratio, free-flow speed ratio and the number of lanes ratio, respectively, of the modified carriageway configuration with respect to the original configuration.

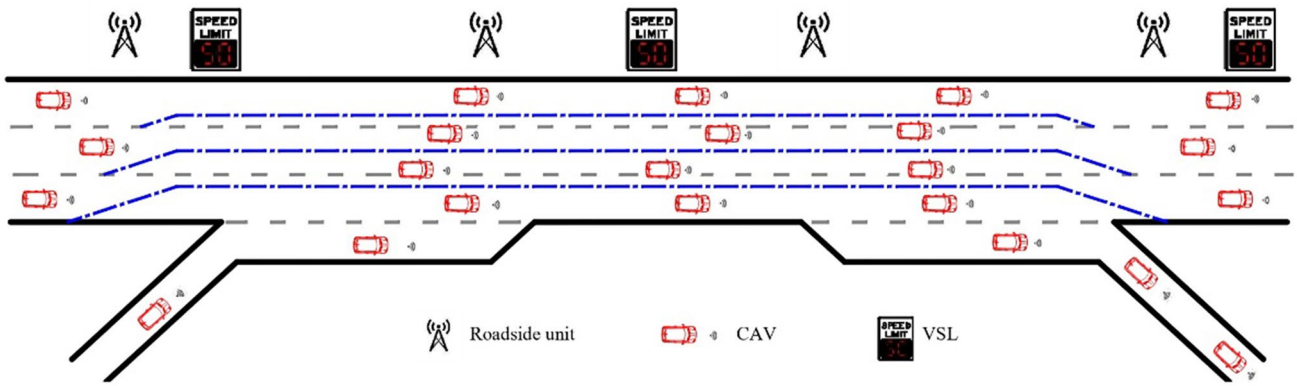

Fig. 12 Smart Road with the integration of DLC system and CAVs (from 3 to 4 lanes per direction and vice versa)

Therefore, the capacity in the changed configuration with a higher number of lanes can be calculated using the following relationship:

$$c_T^{'} = c_T \cdot \gamma \cdot \sigma \cdot \varepsilon \tag{14}$$

Capacity can also be expressed as the reciprocal of the mean time headway (τ_m) between pairs of vehicles in the traffic stream of the carriageway ($c_T = 3600/\tau_m$), so the BPR formula can be rewritten as follows:

$$\begin{aligned} TT &= T_0 \cdot \left[1 + \alpha \left(\frac{q}{c_T^{'}}\right)^{\beta}\right] \\ &= T_0 \cdot \left[1 + \alpha \left(\frac{\tau_m \cdot q}{3600 \cdot \gamma \cdot \sigma \cdot \varepsilon}\right)^{\beta}\right] \end{aligned} \tag{15}$$

This expression is general and therefore allows us to estimate travel time even considering the presence of CAVs in the traffic flow. In fact, starting from a reliable estimate of lane capacity as a function of the percentage of CAVs, i.e., the so-called Market Penetration Level (MPL), we can deduce the value of $\tau_m = 3600/c_T$, which is then introduced into the previous Eq. 14. Given that CAVs technology and regulations are still evolving, certain assumptions are necessary to estimate the potential capacity advantages of CAVs. A central assumption is that these vehicles can operate at significantly shorter time headway distances compared to human-driven vehicles. While autonomous driving systems may technically allow for very small headways, the actual achievable distances will be constrained by several factors, including: a) legal or regulatory requirements that mandate a minimum following distance; b) manufacturer liability concerns, which may lead to more conservative spacing than what is strictly required for safety; and c) passenger comfort considerations, which may limit the acceleration and deceleration needed to maintain close spacing and enable smooth lane changes and merging. This study follows the recommendations provided by the HCM 7th Edition [44]. More precisely, according to the HCM 7th Edition, it is possible to adopt a linear model of the type:

$$\tau_m = A - B \cdot MPL \tag{16}$$

with A and B being the coefficients of the model to be calibrated, and MPL being the percentage of CAVs in traffic flows ($0\% \leq MPL \leq 100\%$).

To calibrate this traffic model, we used the capacity increases proposed by the HCM manual as a function of the MPL, which cover the range of lane capacity values attainable in an urban environment, between 1800 pc/h and 2100 pc/h (Fig. 13a). A linear regression of the suggested capacity values for the entire carriageway (2 lanes) as MPL varies yields the following relationship between the mean time headway and MPL (Fig. 13 b):

$$\tau_m = 0.9283 - 0.0037 \cdot MPL \tag{17}$$

Therefore, the TT can be estimated with Eq. 15, which takes into account the MPL of CAVs.

$$TT = T_0 \cdot \left[1 + \alpha \left(\frac{(0.9283 - 0.0037 \cdot MPL) \cdot q}{3600 \cdot \gamma \cdot \sigma \cdot \varepsilon}\right)^{\beta}\right] \tag{18}$$

Figures14 , 15 and 16 show how the Travel Time (TT) changes as the MPL of CAVs varies. The results were obtained using the previously described closed-form models. More precisely, the following maximum speeds for CAVs were set and imposed in the traffic analyses carried out with the previous equations: $V_{max} = 70$ km/h, $V_{max} = 80$ km/h, and $V_{max} = 90$ km/h. Obviously, the maximum speed V_{max} cannot be maintained consistently along the entire road segment, considering the presence of pedestrian crossings and traffic

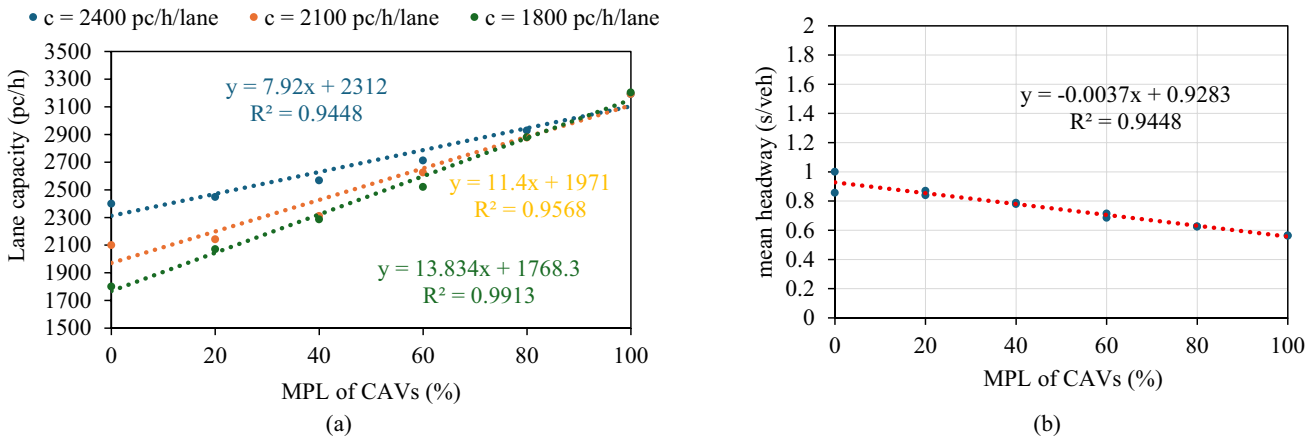

Fig. 13 **a** Lane capacity in function of MPL of CAVs (data from [44]); **b** mean headway in function of MPL of CAVs

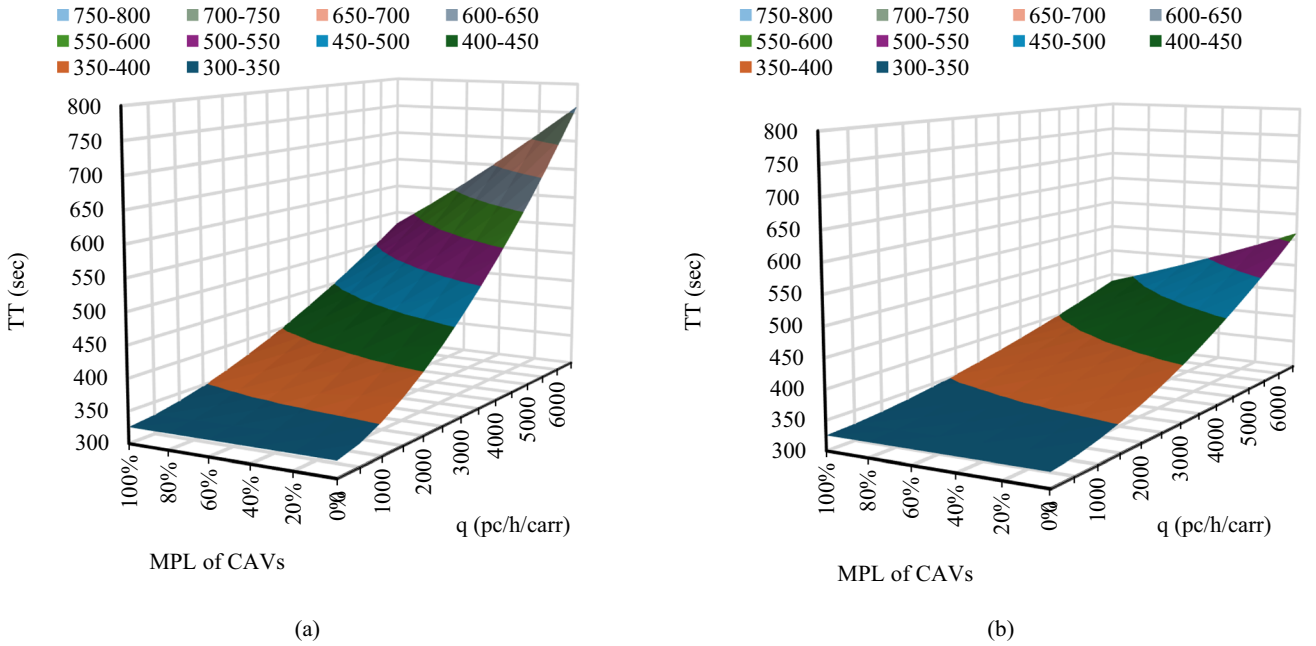

Fig. 14 Travel Time (TT) values as a function of flow (q) and Market Penetration Level of CAVs (MPL) **a** 2 lanes per carriageway; **b** 3 lanes per carriageway. Speed of CAVs, V_{max} = 70 km/h

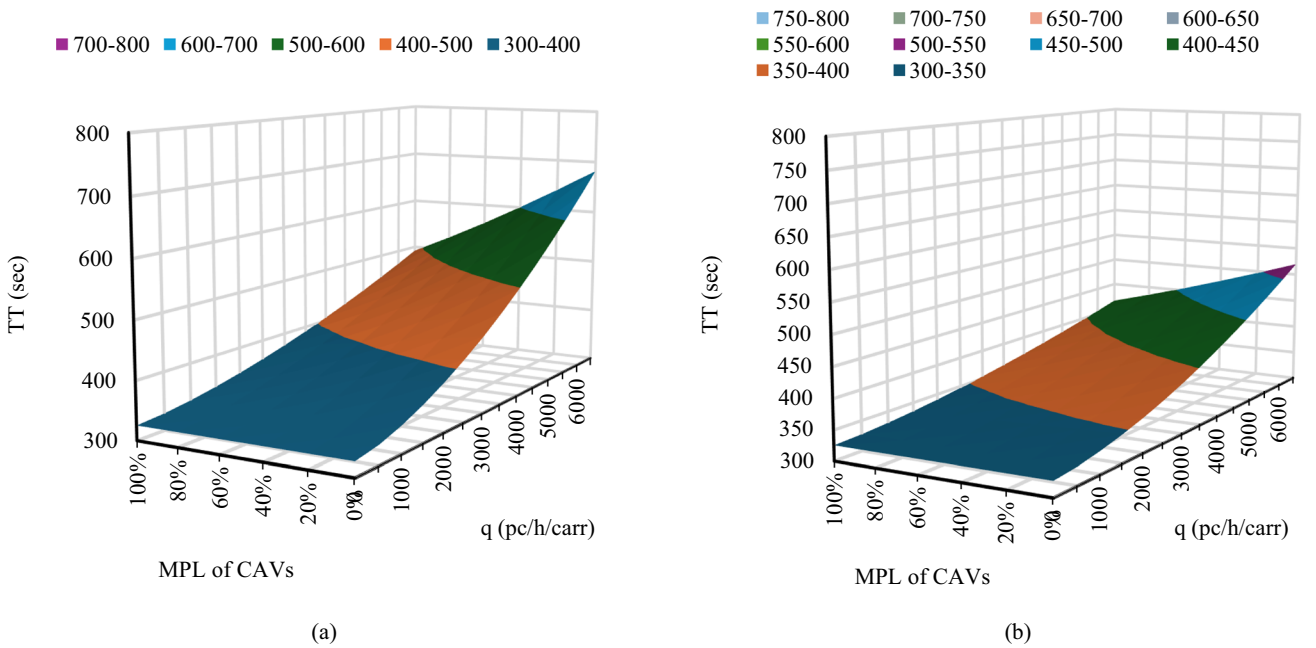

Fig. 15 Travel Time (TT) values as a function of flow (q) and Market Penetration Level of CAVs (MPL) **a** 2 lanes per carriageway; **b** 3 lanes per carriageway. Speed of CAVs, V_{max} = 80 km/h

light intersections. However, it is possible to immediately notice that, with the same vehicular flows q, by varying the percentage of CAVs, a reduction in the TT is obtained and therefore an improvement in the quality of circulation.

Estimating traffic congestion by TT is a crucial component of Intelligent Transport Systems (ITS), designed to enhance control strategies within modern traffic road networks. The analytical relationships of TT previously deduced allow for system optimization. Various strategies can be implemented to ensure a specific minimum LOS value, thereby affecting the vehicle density parameter. Indeed, considering that q = k·v = k·L/TT, where L is the road length section under consideration, the following expression can be deduced:

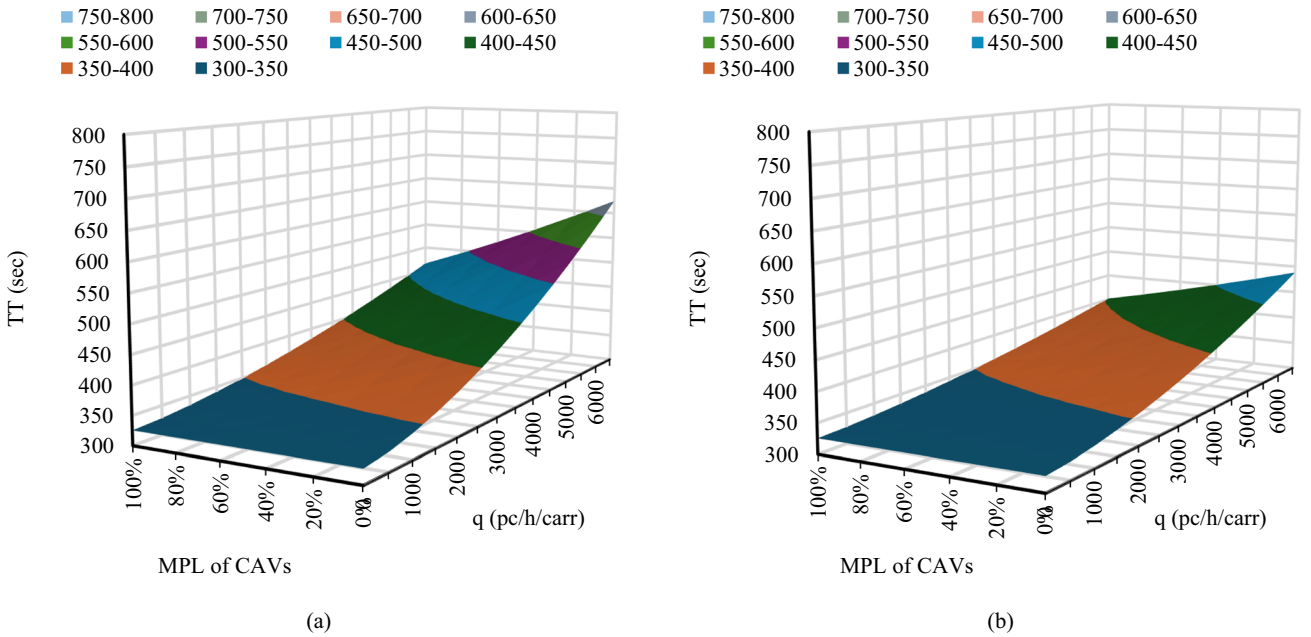

Fig. 16 Travel Time (TT) values as a function of flow (q) and Market Penetration Level of CAVs (MPL) **a** 2 lanes per carriageway; **b** 3 lanes per carriageway. Speed of CAVs, V_{max}=90 km/h

$$k = \frac{q}{L} \cdot T_0 \cdot \left[1 + \alpha \left(\frac{(0.9283 - 0.0037 \cdot MPL) \cdot q}{3600 \cdot \gamma \cdot \sigma \cdot \varepsilon} \right)^{\beta} \right] \quad (19)$$

in which L is the length of the analysed arterial segment.

The desirable limit density value can be set ($k \leq k_{lim}$) as follows:

$$k = \frac{q}{L} \cdot T_0 \cdot \left[1 + \alpha \left(\frac{(0.9283 - 0.0037 \cdot MPL) \cdot q}{3600 \cdot \gamma \cdot \sigma \cdot \varepsilon} \right)^{\beta} \right] \leq k_{lim} \quad (20)$$

In Eq. 20, the values of k_{lim} are the following: k_{lim}=7 pc/km for LOS A, k_{lim}=11 pc/km for LOS B, k_{lim}=16 pc/km for LOS C, k_{lim}=22 pc/km for LOS D, k_{lim}=28 pc/km for LOE A, k_{lim}>28 pc/km for LOS F. So, for a given value of q, by acting on one or more of the variables ?, ?, ?, the traffic density and therefore the LOS can be maintained under the desirable limit. For example, the number of lanes can be increased by adjusting the variable ε, while keeping all other conditions unchanged. Alternatively, the speed of the CAVs can be modified by changing the variable σ with the number of lanes remaining constant, or both factors can be adjusted simultaneously. It is also possible to evaluate the expected benefits of the DLC traffic regulation system in terms of the Travel Time Index (TTI=TTI(q)). The traffic analysis results (Figs. 17, 18 and 19) show that the TTI values clearly tend to decrease in the 3-lane configuration, and for a given flow q, decrease as the MPL of CAVs increases. A comparison of the values in Figs. 10 and 17, 18 and 19 shows that the TTIs estimated for the case of DLC active even during peak hours are always lower than TTI=2, except cases of exceptionally high flow q (q>5500 pc/h/carr), 2-lane configuration and V_{max}=70 km/h, where TTI>2 occurs (Fig. 17a). The benefits become increasingly more marked as the speed Vmax increases. In fact, for V_{max}=90 km/h and 3 lanes per carriageway, even in the most critical traffic conditions (i.e. up to q=6500 pc/h/carr), the TTI=1.5 is never exceeded (Fig. 19 b). Additional benefits can potentially be obtained by combining lane-free artificial-fluid lane-free traffic (i.e., the DLC) with the "nudging" traffic regulation system, whereby CAVs influence other vehicles in front of or beside them [50, 56]. This aspect can be considered in future studies.

Conclusions

To mitigate congestion on urban and suburban road networks, specific capacity-enhancement strategies must be implemented, either through physical and structural interventions or by adopting suitable traffic regulation systems. The advent of smart roads and Connected and Autonomous Vehicles (CAVs) offers new opportunities to enhance road performance by adapting capacity to fluctuating traffic demand over time. Among these strategies, Dynamic Lane Configuration (DLC) enables the flexible adjustment of the number and width of lanes, without compromising

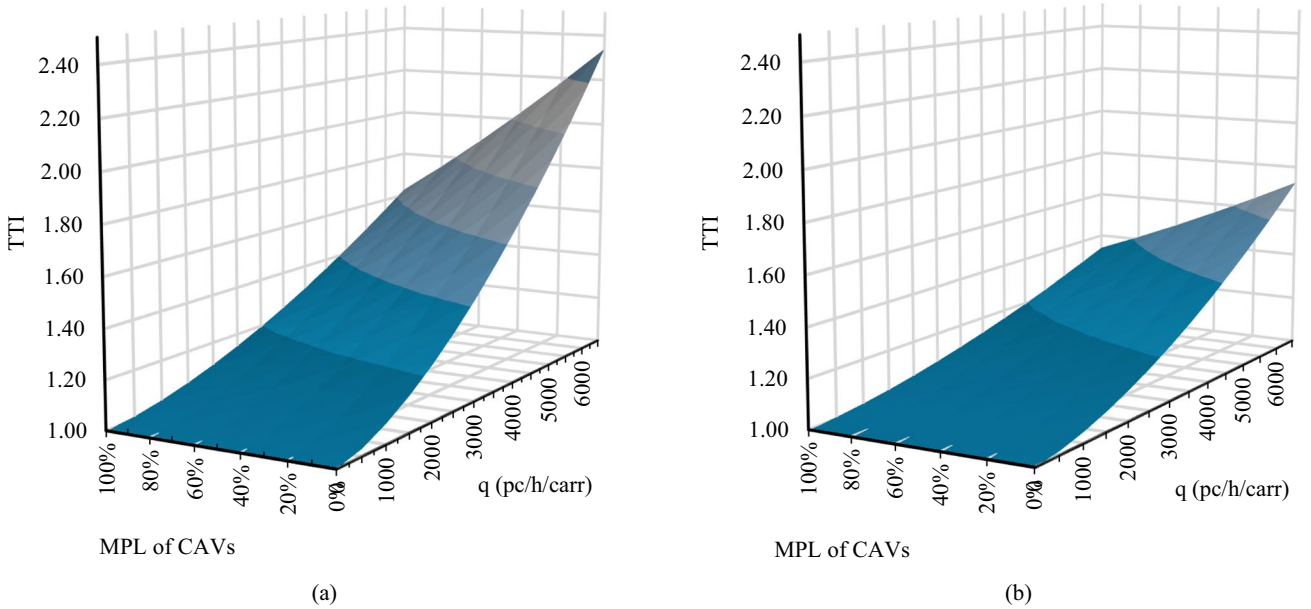

Fig. 17 Travel Time Index values as a function of flow (q) and Market Penetration Level of CAVs (MPL) **a** 2 lanes per carriageway; **b** 3 lanes per carriageway. Speed of CAVs, Vmax = 70 km/h

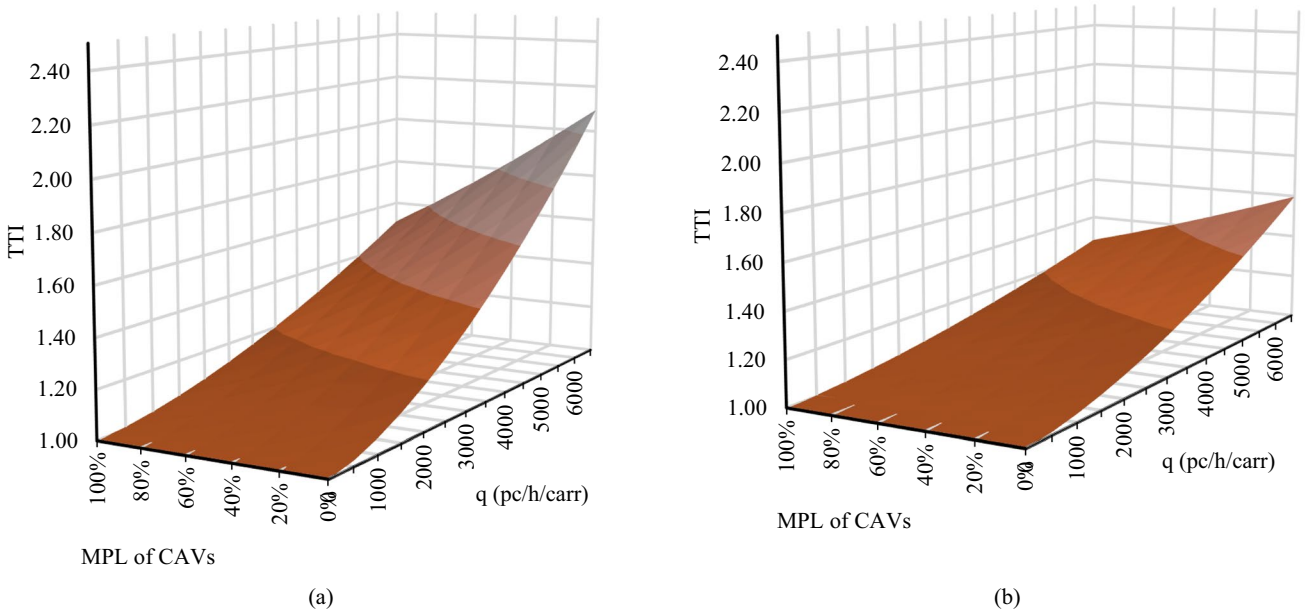

Fig. 18 Travel Time Index values as a function of flow (q) and Market Penetration Level of CAVs (MPL) **a** 2 lanes per carriageway; **b** 3 lanes per carriageway. Speed of CAVs, V_{max} = 80 km/h

road safety, in traffic flows that include CAVs. This paper presents the results of a study conducted on an urban arterial road (i.e., Viale Regione Siciliana) in Palermo, Italy. It highlights the importance of adopting a holistic approach based on emerging innovative transportation technologies to alleviate urban congestion problems. The results of this research should, however, be considered provisional, as numerous practical constraints currently exist (e.g., the large-scale implementation of CAVs, the introduction of specific technical regulations, the calibration and validation of traffic regulation systems, accident forecasts, and economic constraints related to the implementation of innovative traffic regulation systems).

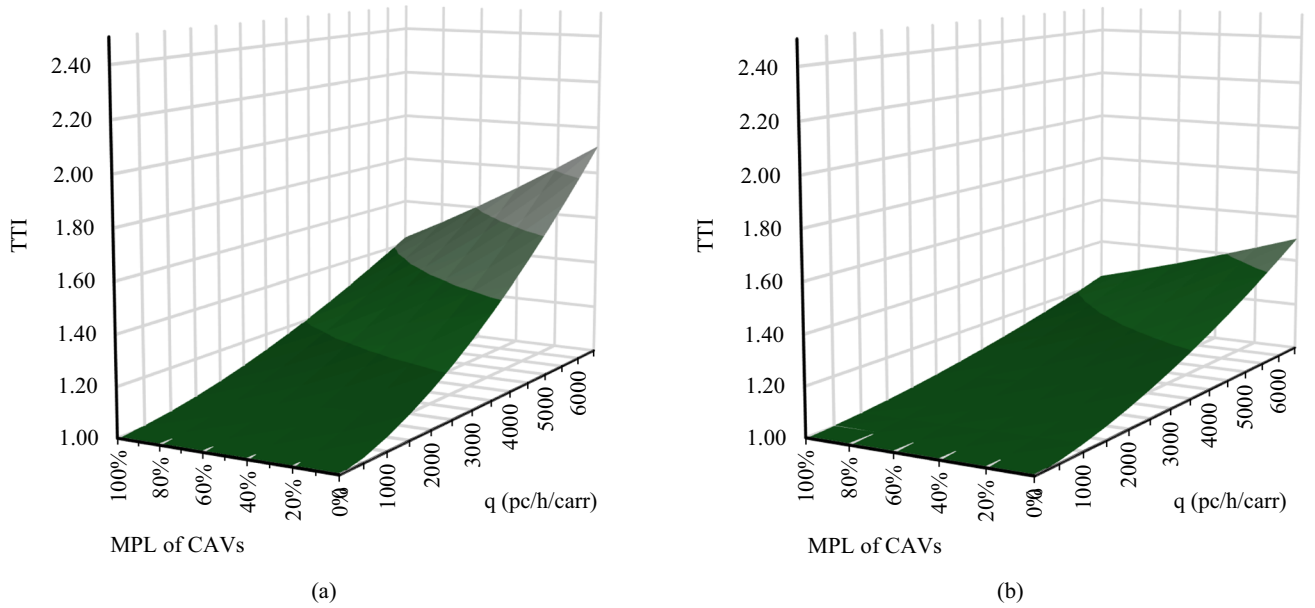

Fig. 19 Travel Time Index values as a function of flow (q) and Market Penetration Level of CAVs (MPL) **a** 2 lanes per carriageway; **b** 3 lanes per carriageway. Speed of CAVs, V_{max} = 90 km/h

Major findings of the study

Travel times and space mean speeds were collected through the analysis of TomTom big data; Macroscopic Fundamental Diagrams (MFDs) and travel time functions were deduced in the case of manually driven vehicles by comparing two very different lane configurations (two lanes per direction versus three lanes per direction). In addition, a relatively simplified closed-form traffic engineering model, based on the well-known BPR function, was subsequently formulated to evaluate the effects of implementing DLC on the selected roadway, with a view toward its potential transformation into a smart road that accommodates varying Market Penetration Levels of CAVs in the future.

The traffic flow of CAVs is conceived as an artificially designed fluid: its collective properties are programmable and optimizable primarily in terms of maximum speeds (V_{max}) that should not be exceeded. The proposed approach was then tested through a series of traffic analyses, considering numerous traffic demand levels, by varying the flow q. Three different maximum speed limits were imposed on CAVs: V_{max} = 70 km/h, V_{max} = 80 km/h, and V_{max} = 90 km/h. In all the tested conditions, the traffic regulation systems demonstrated the potential benefits of this innovative traffic management strategy. In fact, the outcomes indicated that when the DLC forces CAVs to deploy in three lanes, rather than the original two lanes, TTs are significantly reduced. Furthermore, an optimal control approach was proposed to determine the timing and location for implementing a new lane configuration, based on acceptable density thresholds.

Limitations of the study

This research has several limitations that are encountered at various stages. First, the study relies entirely on TomTom FCD and on sample flow measurements in some road sections due to the lack of other traffic survey systems (e.g. loops and radars) on the examined arterial road. A significant limitation is that the dynamic lane configuration is still in the conceptual stage of development, and CAVs are not yet a traffic component on which experimental data can be obtained. In addition, for the sake of simplicity in this study, the one-regime Greenshields model has been employed to estimate the macroscopic fundamental diagrams. Finally, the BPR model sometimes results in inadequate predictions of travel time on congested urban arterials, such as those analysed in this research, during peak traffic hours.

Research perspectives

Smart Roads, CAVs, and DLCs, as integral components of transportation systems and traffic control strategies, can be effectively integrated to enhance overall road network performance by dynamically adjusting capacity in response to varying traffic demand levels. Despite the promising results obtained by combining these innovative systems, future research must investigate the safety implications of mixed CAVs and HDVs flow conditions, which remain largely unexplored. Furthermore, future research could utilise more accurate macroscopic flow models and travel time estimation equations to better account for the effects of potential

congestion on urban arterial roads, as well as through sensitivity analysis performed on key traffic parameters. Finally, traffic microsimulation models could be implemented to estimate headway reductions, platooning formation, and vehicle lateral positioning, precisely the mechanisms through which CAVs would affect DLC performance even in cases of adverse weather conditions, accidents or road works.

Funding Open access funding provided by Università degli Studi di Trento within the CRUI-CARE Agreement.

Declarations

Conflict of interest The authors declare that they have no known competing financial interests or personal relationships that could have appeared to influence the work reported in this paper.

Ethical approval This study did not involve any human participants, animals, or clinical trials. Therefore, ethical approval was not required.

Informed consent Not applicable. This research does not include any human subjects or identifiable personal data.

Open Access This article is licensed under a Creative Commons Attribution 4.0 International License, which permits use, sharing, adaptation, distribution and reproduction in any medium or format, as long as you give appropriate credit to the original author(s) and the source, provide a link to the Creative Commons licence, and indicate if changes were made. The images or other third party material in this article are included in the article's Creative Commons licence, unless indicated otherwise in a credit line to the material. If material is not included in the article's Creative Commons licence and your intended use is not permitted by statutory regulation or exceeds the permitted use, you will need to obtain permission directly from the copyright holder. To view a copy of this licence, visit http://creativecommons.org/licenses/by/4.0/.

References

1. Chou C-C, Chiang W-C, Chen AY (2022) Emergency medical response in mass casualty incidents considering the traffic congestions in proximity on-site and hospital delays. Transport Res Part E: Logist Transport Rev 158:102591. https://doi.org/10.1016/j.tre.2021.102591
2. X Kong, J Yang, Z Yang (2015) Measuring Traffic Congestion with Taxi GPS Data and Travel Time Index, In: CICTP 2015, Beijing, China: American Society of Civil Engineers, July 2015, pp. 3751–3762. https://doi.org/10.1061/9780784479292.346.
3. Bhouri N, Aron M, Scemama G (2016) Travel time reliability with and without the dynamic use of hard shoulder: Field assessment from a French motorway. J Traffic Transport Eng (English Edition) 3(6):520–530. https://doi.org/10.1016/j.jtte.2016.01.008
4. Peng R, Yang M, Han Y, Zhang R, Zhang M (2025) Control strategy of hard shoulder running at intelligent freeway merging areas based on deep reinforcement learning. IEEE Trans Veh Technol 74(9):13642–13657. https://doi.org/10.1109/TVT.2025.3559227
5. Fitzpatrick K, Dixon K, Avelar R (2016) Evaluating operational implications of reduced lane and shoulder widths on freeways. J Transp Eng 142(11):04016052. https://doi.org/10.1061/(ASCE)TE.1943-5436.0000884
6. Pokorny P, Jensen JK, Gross F, Pitera K (2020) Safety effects of traffic lane and shoulder widths on two-lane undivided rural roads: a matched case-control study from Norway. Accid Anal Prev 144:105614. https://doi.org/10.1016/j.aap.2020.105614
7. Zegeer CV, Deen RC, Mayes JG, (1980) Effect of lane and shoulder widths on accident reduction on rural, two-lane roads', *Trans Res Record J Trans Res Board*, [Online]. Available: http://onlinepubs.trb.org/Onlinepubs/trr/1981/806/806-006.pdf
8. CG Cassandras, AS Chavez Armijos, A Li, E Sabouni (2024) Automated Mobility and Cooperation Compliance in Mixed Vehicle Traffic Environments', In: Transportation Mobility in Smart Cities, vol. 21, P Ioannou, AA Malikopoulos, Eds, in Springer Tracts on Transportation and Traffic, vol. 21. , Cham: Springer Nature Switzerland, pp. 25–53. https://doi.org/10.1007/978-3-031-64769-7_2.
9. Guerrieri M et al (2012) A theoretical and experimental approach to reconstructing the transverse profile of worn-out rails. Ingegneria Ferroviaria 67(1):23–37
10. Khanmohamadi M, Guerrieri M (2024) Advanced sensor technologies in cavs for traditional and smart road condition monitoring: a review. Sustainability 16(19):8336. https://doi.org/10.3390/su16198336
11. Owais M, Alshehri A (2020) Pareto optimal path generation algorithm in stochastic transportation networks. IEEE Access 8:58970–58981. https://doi.org/10.1109/ACCESS.2020.2983047
12. Almutairi A, Owais M (2025) Reliable vehicle routing problem using traffic sensors augmented information. Sensors 25(7):2262. https://doi.org/10.3390/s25072262
13. Li P, Chen Y, Hu Y, Shi J, Li K, Luo Y (2025) Collaborative multi-lane scheduling strategy for connected and automated vehicles on highway interchange using rolling traversal scheduling. Comput Aid Civil Eng 40(30):6127–6148. https://doi.org/10.1111/mice.70141
14. Amoei Khorshidi N, Afandizadeh Zargari S, Mirzahossein H, Shakoori S, Jin X (2025) Modeling suburban freeway travel variability considering connected and autonomous vehicles. Int J Civ Eng 23(3):419–442. https://doi.org/10.1007/s40999-024-01045-1
15. W. Zhang *et al.*, (2025) A cooperative lane-changing control method for connected and autonomous vehicles in expressway diversion area considering dedicated lanes, J Intell Transport Syst pp. 1–18, https://doi.org/10.1080/15472450.2025.2531351.
16. Gajera H, Pulugurtha SS, Gore N, Ghasemi A, Duvvuri S, Kodupuganti SR (2025) Modeling and estimating the effect of a mix of varying levels of automated vehicles on operational performance of urban freeways. Transp Res Rec 2679(3):1054–1075. https://doi.org/10.1177/03611981241287195
17. Guerrieri M (2021) Smart roads geometric design criteria and capacity estimation based on AV and CAV emerging technologies. A case study in the Trans-European Transport Network. Int J ITS Res 19(2):429–440. https://doi.org/10.1007/s13177-021-00255-4
18. Guerrieri M, Parla G, Khanmohamadi M, Neduzha L (2024) Asphalt pavement damage detection through deep learning technique and cost-effective equipment: a case study in urban roads crossed by tramway lines. Infrastructures 9(2):34. https://doi.org/10.3390/infrastructures9020034
19. Gore N, Arkatkar S, Joshi G, Pulugurtha SS (2023) A hazard-based model to derive travel time under congested conditions. Transp Policy 138:1–16. https://doi.org/10.1016/j.tranpol.2023.05.003
20. Gore N, Arkatkar S, Joshi G, Antoniou C (2023) Modified bureau of public roads link function. Transp Res Rec 2677(5):966–990. https://doi.org/10.1177/03611981221138511
21. Mtoi ET, Moses R (2014) Calibration and evaluation of link congestion functions: applying intrinsic sensitivity of link speed as a practical consideration to heterogeneous facility types within urban network. JTTs 04(02):141–149. https://doi.org/10.4236/jtts.2014.42014

22. Alsobky A, Darwish AM (2023) A realistic framework for volume-delay function determination. Ain Shams Eng J 14(12):102279. https://doi.org/10.1016/j.asej.2023.102279
23. Rose G, Taylor MAP, Tisato P (1989) Estimating travel time functions for urban roads: options and issues. Transp Plan Technol 14(1):63–82. https://doi.org/10.1080/03081068908717414
24. Pulugurtha SS, Imran MS (2021) Average travel time, planning time index, and buffer time index thresholds for freeway weaving sections, merging areas, and diverging areas. J Transp Eng, Part A: Syst 147(9):04021051. https://doi.org/10.1061/JTEPBS.0000549
25. Spiess H (1990) Technical note—conical volume-delay functions. Transp Sci 24(2):153–158. https://doi.org/10.1287/trsc.24.2.153
26. Akcelik R (1991) Travel time functions for transport planning purposes: Davidson's function, its time-dependent form and an alternative travel time function. Australian Road Research, 21(3).
27. L Elefteriadou (2024) *An Introduction to Traffic Flow Theory*, vol. 84. in Springer Optimization and Its Applications, vol. 84. Cham: Springer International Publishing. https://doi.org/10.1007/978-3-031-54030-1.
28. Ebeling CE (1997) An introduction to reliability and maintainability engineering. McGraw Hill, New York
29. Wang J, Wang C, Lv J, Zhang Z, Li C (2017) Modeling travel time reliability of road network considering connected vehicle guidance characteristics indexes. J Adv Transp 2017:1–9. https://doi.org/10.1155/2017/2415312
30. Sun Y, Chen Y (2024) Travel time variability in urban mobility: exploring transportation system reliability performance using ridesharing data. Sustainability 16(18):8103. https://doi.org/10.3390/su16188103
31. Chen Z, Fan W (2019) Data analytics approach for travel time reliability pattern analysis and prediction. J Mod Transp 27(4):250–265. https://doi.org/10.1007/s40534-019-00195-6
32. Travel time reliability: making it there on time, all the time. FHWA report. U.S. Federal Highway Administration (FHWA), (2006).
33. Pu W (2011) Analytic relationships between travel time reliability measures. Transport Res Record: J Transport Res Board 2254(1):122–130. https://doi.org/10.3141/2254-13
34. Lomax T *et al.* (1997) Quantifying congestion. volume 1: Final report. [Online]. Available: http://onlinepubs.trb.org/onlinepubs/nchrp/nchrp_rpt_398.pdf
35. California Department of and Transportation, (1998) California Transportation Plan: transportation system performance measures: final report.
36. Texas Transportation Institute (2008) Costeffective performance measures for travel time delay, variation, and reliability. NCHRP report 618'.
37. Van Lint JWC, Van Zuylen HJ (2005) Monitoring and predicting freeway travel time reliability: using width and skew of day-to-day travel time distribution. Transport Res Record: J Transport Res Board 1917(1):54–62. https://doi.org/10.1177/0361198105191700107
38. Dowling, Richard G, Skabardonis, Alexander, Margiotta, Richard A, Hallenbeck, Mark E, (2009) 'Reliability Breakpoints on Freeways', In: TRB 88th Annual Meeting Compendium of Papers DVD.
39. Willumsen L (2021) Use of Big Data in Transport Modelling', International Transport Forum Discussion Papers 2021/05. https://doi.org/10.1787/86a128c7-en.
40. Salvo G, Karakikes I, Papaioannou G, Polydoropoulou A, Sanfilippo L, Brignone A (2025) Enhancing urban resilience: managing flood-induced disruptions in road networks. Transport Res Interdiscipl Perspect 31:101383. https://doi.org/10.1016/j.trip.2025.101383
41. Pozzoni M, Ceccarelli G, Gorrini A, Manenti L, Sanfilippo L (2023) TomTom data applications for the assessment of tactical urbanism interventions: the case of Bologna. Sustainability 15(17):12716. https://doi.org/10.3390/su151712716
42. Comune di Palermo (2010) 'Piano generale del traffico urbano(PGTU)'. [Online]. Available: https://repository.comune.palermo.it/amministrazione-trasparente.php?grp=3%26lev=4%26id=168
43. HCM (2010) highway capacity manual, 5th edn. Transportation Research Board, Washington, D.C., p 2010
44. E. National Academies of Sciences, (2022) Highway Capacity Manual 7th Edition: A Guide for Multimodal Mobility Analysis. Washington, D.C: National Academies Press.
45. *TRNews*. Washington, D.C.: National Academies Press, 2000, p. 895. https://doi.org/10.17226/895.
46. Gore N, Arkatkar S, Joshi G, Antoniou C (2023) Modified bureau of public roads link function. Transport Res Record: J Transport Res Board 2677(5):966–990. https://doi.org/10.1177/03611981221138511
47. Kniz A, Kocianova A (2023) Analysis in the field of volume-delay function research. Transp Res Procedia 74:1022–1029. https://doi.org/10.1016/j.trpro.2023.11.239
48. Gu J, Yu L, Li M (2020) Application study on urban road volume-time function based on RFID data. IOP Conf Ser Mater Sci Eng 787(1):012018. https://doi.org/10.1088/1757-899X/787/1/012018
49. Rostami-Shahrbabaki M, Keyvan-Ekbatani M, Bogenberger K, Papageorgiou M (2025) Dynamic lane configuration for improved traffic efficiency on motorways. IEEE Trans Intell Transp Syst. https://doi.org/10.1109/TITS.2025.3592304
50. M. Papageorgiou *et al* (2024) Highlights of Lane-Free Automated Vehicle Traffic with Nudging. In: Transportation Mobility in Smart Cities, vol. 21, P Ioannou, AA Malikopoulos, Eds, in Springer Tracts on Transportation and Traffic, vol. 21. , Cham: Springer Nature Switzerland, pp. 147–183. https://doi.org/10.1007/978-3-031-64769-7_6.
51. M Guerrieri, M Khanmohamadi (2025) COM-Roundabout: The first smart commutable and self-regulating roundabout for HDVs and CAVs, Int J Transport Sci Technol, p. S2046043025000541, https://doi.org/10.1016/j.ijtst.2025.04.003.
52. Guerrieri M, Khanmohamadi M (2025) SSF-roundabout: a smart and self-regulated roundabout with right-turn bypass lanes. Appl Sci 15(16):8971. https://doi.org/10.3390/app15168971
53. HA Al Hasanat, O Alharasees, D Alothman (2024) Connected Automated Vehicles Entry Capacity on Roundabouts- Case Study Hungary, In: 2024 2nd International Conference on Technology Innovation and Its Applications (ICTIIA), Medan, Indonesia: IEEE, pp. 1–6. https://doi.org/10.1109/ICTIIA61827.2024.10761405.
54. Hasanat HAA, Alharasees O (2025) The influence of geometry and connected automated vehicles on single-lane roundabout capacity. Innov Infrastruct Solut 10(9):412. https://doi.org/10.1007/s41062-025-02226-0
55. Khadka N, Hassan H (2025) Exploring the effects of connected and autonomous vehicles on traffic safety and operation at full-cloverleaf interchanges. J Transp Saf Secur 17(1):1–29. https://doi.org/10.1080/19439962.2024.2361150
56. Papageorgiou M, Mountakis K-S, Karafyllis I, Papamichail I, Wang Y (2021) Lane-free artificial-fluid concept for vehicular traffic. Proc IEEE 109(2):114–121. https://doi.org/10.1109/JPROC.2020.3042681

Publisher's note Springer Nature remains neutral with regard to jurisdictional claims in published maps and institutional affiliations.